Available online at www.sciencedirect.com
SCIENCE DIRECT®
Acta Materialia 52 (2004) 607–614
Acta MATERIALIA
www.actamat-journals.com

Molecular dynamics simulation of screw dislocations interacting with interstitial frank loops in a model FCC crystal

David Rodney *

Génie Physique et Mécanique des Matériaux (UMR CNRS 5010), Institut National Polytechnique de Grenoble, ENSPG, 101 rue de la Physique, Saint Martin d'Hères Cedex BP 46 38402, France

Received 1 July 2003; received in revised form 29 September 2003; accepted 29 September 2003

Abstract

Molecular dynamics simulations of screw dislocations interacting with interstitial Frank loops are performed using specific boundary conditions in a model face-centered-cubic nickel crystal, in a configuration favorable to the formation of a helical turn on the dislocation. Both the interaction mechanism and the pinning stress caused by the defects are studied. In particular, we show (1) that the interactions involve athermal cross-slip events, (2) that the shape of the loop has a strong influence: loops with edges along $\langle 1\,1\,0\rangle$ directions are unfaulted while loops with $\langle 1\,2\,1\rangle$ edges are just sheared and (3) that the Frank loops are strong obstacles with unpinning reactions involving Orowan processes. The consequences of these observations on clear band formation are discussed.

Keywords: Molecular dynamics; Dislocation; Irradiation; Frank loops

1. Introduction

Neutron irradiations in face-centered-cubic (FCC) materials produce defect clusters made of either interstitials in the case of black dots and Frank loops or vacancies in the case of stacking fault tetrahedra (SFT). The respective densities of these defects depend on the material and the irradiation conditions. In particular, at low temperatures (typically below 300 °C $\sim 0.3T_M$), black dots and Frank loops are mainly observed in austenitic steels whereas the irradiation microstructure is dominated by SFT's in copper and, in nickel, there is a crossover from a SFT dominated microstructure at low dose (typically below 0.01 dpa) to a Frank loop dominated microstructure at higher doses (for reviews, see, for example [1,2] for Cu and Ni, [3,4] for austenitic steels).

Irradiation defects cause a degradation of the mechanical properties with an increase of the yield stress, a decrease of the ductility and, beyond a certain dose level, softening and plastic flow localization in bands which are clear of irradiation defects after deformation and are thus called 'clear bands' (for reviews, see, for example [5] for mechanical properties and [6,7] for clear bands).

In the case of austenitic steels, clear band formation is usually attributed to the unfaulting of the Frank loops: interaction with the mobile lattice dislocations removes the fault of the Frank loops which are transformed into perfect loops that may then be eliminated by prismatic glide or drag by the moving dislocations [6]. Frank loops and their interactions with dislocations have, up to now, been studied using transmission electron microscopy (TEM) mainly in the case of quenched metals (for example [8]) where the loops are made by the condensation of vacancies. Their intrinsic fault is removed when swept by a single Shockley partial, according to the classical reaction [9],

$$\frac{a}{3}[1\,1\,1]+\frac{a}{6}[1\,1\,\bar{2}]\rightarrow\frac{a}{2}[1\,1\,0]. \quad (1)$$

By way of contrast, in irradiated materials, Frank loops are made of interstitials. Their extrinsic fault is made of two stacking faults on adjacent $\{1\,1\,1\}$ planes and their removal requires sweeping by two Shockley partials. The usual Burgers vector reaction (Eq. (1)) remains valid but the $a/6[1\,1\,\bar{2}]$ partial is now made of two partials on adjacent $\{1\,1\,1\}$ planes according to

* Tel.: +33-476 826-337; fax: +33-474-826-382.
E-mail address: david.rodney@gpm2.inpg.fr (D. Rodney).

1359-6454/$30.00 © 2003 Acta Materialia Inc. Published by Elsevier Ltd. All rights reserved.
doi:10.1016/j.actamat.2003.09.044

$$\frac{a}{6}[1\,1\,\bar{2}] \rightarrow \frac{a}{6}[2\,\bar{1}\,\bar{1}] + \frac{a}{6}[\bar{1}\,2\,\bar{1}]. \quad (2)$$

The cores of the two partials may be separated, but they may also join, forming a single core extended over 2 {1 1 1} planes. In this case, the dislocation is called a D-Shockley partial [10]. Indeed, Suzuki et al. [11], studying by TEM proton-irradiated steels, observed dislocations adjoining Frank faults with a single contrast consistent with D-type partials. However, this study offered no details on the dislocation/loop interaction mechanisms. Recently, Robach et al. [12] used in-situ TEM to observe dislocation motion in heavy-ion irradiated Cu specimens and computed directly from the images the distribution of pinning stresses due to the irradiation defects. But again, the TEM observations gave no microscopic detail on the interaction mechanisms.

In order to better understand the interactions between dislocations and Frank loops, we have undertaken a systematic investigation by molecular dynamics (MD) of all the possible configurations between edge and screw dislocations interacting with interstitial Frank loops. We use nickel as a prototypical FCC material. MD simulations of dislocations interacting with irradiation defects have, up to now, focused on edge dislocations. The irradiation defects considered were glissile interstitial loops of the type that form in MD simulations of displacement cascades in an FCC nickel crystal [13], stacking fault tetrahedra in an FCC copper crystal [14] and voids and second phase precipitates in a BCC iron crystal [15].

We present here results concerning a screw dislocation interacting with a Frank loop lying in a {1 1 1} plane that is *not* a cross-slip plane for the dislocation. This configuration is favorable to the formation of a so-called 'helical turn' on the dislocation line. It is only one particular geometry out of all the possible configurations. However, it shows complex reactions that deserve a detailed analysis and requires the use of specific boundary conditions adapted to screw dislocations. The other configurations, involving also edge dislocations, will be presented in a future paper.

The outline of the paper is the following. In Section 2, we present boundary conditions adapted to the MD simulation of screw dislocations. In Section 3, we focus on the interaction mechanism and evaluate the pinning stress due to this defect. In Section 4, we discuss the implications of our simulations in particular with respect to the dynamics of clear band formation.

2. Simulation technique

2.1. Simulation cell and boundary conditions

We present here the main characteristics of the MD simulations which are adapted from those detailed in [13] and allow the simulation of screw dislocations in an infinite periodic glide plane.

We use the embedded atom method potential developed by Angelo et al. [16] to simulate dislocations in nickel crystals. The simulation cell is sketched in Fig. 1 along with a Thompson tetrahedron showing the crystallographic orientation. Throughout this paper, notations for Burgers vectors are taken according to this tetrahedron. Greek letters are used to label the center of the face opposite to the corresponding Latin letter.

The crystallographic orientation was chosen such that a perfect screw $a/2[1\,1\,0](1\,1\,1)$ dislocation may be introduced between the two central $(1\,\bar{1}\,1)$ planes of the cell, with a line along the central $Y = [1\,1\,0]$ axis and a **CA** Burgers vector. Three cells are used with same dimensions in the X and Z directions (21.6×15.7 nm^2) and a varying dimension in the Y-direction (small: 20.0 nm; medium: 37.3 nm and large: 59.7 nm) in order to study the influence of the spacing between defects on the unpinning stress of the dislocation. The cells contain respectively 0.63, 1.17 and 1.87 million atoms.

We use boundary conditions that allow constructing an infinite periodic glide plane for the screw dislocation. Fig. 2 is a detail of the simulation cell seen from above, in the negative Z-direction. The gray lines are the traces of six (1 1 0) planes in an undeformed crystal. For the sake of clarity, only one every two (1 1 0) planes constituting the periodicity in this direction is shown. A

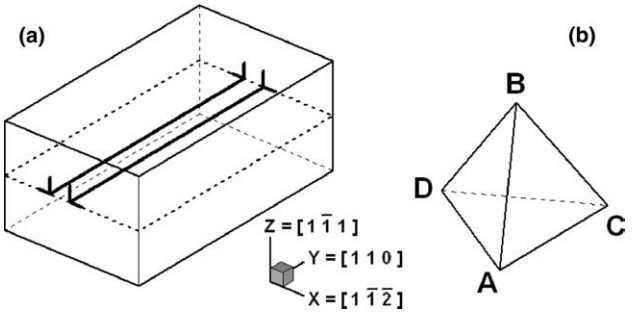

Fig. 1. Sketch of the simulation cell (a) and associated Thompson tetrahedron (b).

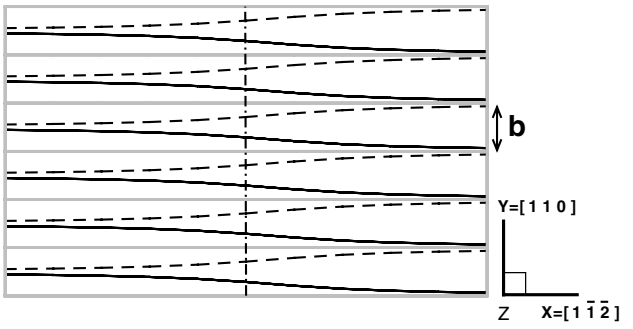

Fig. 2. Traces of (1 1 0) planes before (gray lines) and after (solid and dashed lines) introduction of a screw dislocation along the dashed dotted line.

screw dislocation is introduced along the dash-dotted line, in the Y-direction, by means of its elastic displacement field. The solid and dashed lines are the traces of the $(1\,1\,0)$ planes in the upper (solid) and lower (dashed) $(1\,\bar{1}\,1)$ surfaces of the cell after application of the dislocation displacement field.

Periodicity in the Y-direction is insured by the invariance of the displacement field in this direction. In the X-direction, we use periodic boundary conditions along with a shift of $+b/2$ in the Y-direction for atoms leaving the cell from the left hand negative surface and reintroduced on the right-hand positive surface, and an opposite shift of $-b/2$ for atoms moving in the opposite direction. The reason is that, as shown in Fig. 2, the $(1\,1\,0)$ planes turn around the dislocation line and arrive with a shift of $b/2$ in the two opposite $(1\,\bar{1}\,\bar{2})$ surfaces. Application of the above boundary condition brings into continuity both sides of the $(1\,1\,0)$ planes, thus reconstructing a periodic glide plane.

The $(1\,1\,0)$ planes are inclined in the $(1\,\bar{1}\,\bar{2})$ surfaces. This is visible in Fig. 2 from the fact that the upper and lower traces of the planes (solid and dashed lines in Fig. 2) do not arrive at the same position on the $(1\,\bar{1}\,\bar{2})$ surfaces, but are distant of $b\cdot\tan^{-1}(L_z/L_x)/\pi$. Application of the above boundary conditions forces the $(1\,1\,0)$ planes to be vertical in the $(1\,\bar{1}\,\bar{2})$ surfaces. Therefore, the influence of the boundary conditions will be minimized by choosing a simulation cell with a small L_z/L_x ratio which minimizes the initial inclination of the $(1\,1\,0)$ planes in the $(1\,\bar{1}\,\bar{2})$ surfaces.

Finally, in the Z-direction, we apply modified free boundary conditions: atoms lying in the upper and lower $(1\,\bar{1}\,1)$ surfaces are constrained to two-dimensional dynamics and are fixed in the Z-direction. Similar conditions have been used in [13] and allow for atomic relaxations inside the surfaces both when the dislocation is at rest and when it moves in its glide plane.

A constant shear stress σ_{yz} may be applied by superimposing constant and opposite forces in the $Y=[1\,1\,0]$ direction to the forces felt by the atoms in the upper and lower $(1\,\bar{1}\,1)$ surfaces. Strong inertial effects are observed in the MD simulations, with the dislocation first overpassing its equilibrium position, then oscillating around the latter with periods of the order of 10 ps. We found that the following methodology minimizes the influence of these inertial effects on the evaluation of the critical unpinning stresses: we first perform a series of Molecular Static simulations by conjugate gradient minimizations with stress increments of 75 MPa in order to bracket the unpinning stress. Starting from the highest stress before unpinning, we then perform MD simulations with again stress increments of 75 MPa and 30 ps between increments.

Time is integrated using Verlet algorithm with a time step of 2×10^{-15} ps and an initial temperature after equilibration of 100 K. No temperature control is needed because the dislocations glide over limited distances and the applied stress produces little work. In practice, the temperature remained below 105 K during all simulations.

2.2. Frank loops

The interstitials forming the Frank loops are inserted 'by hand' in the simulation cell between two $\{1\,1\,1\}$ planes. An initial conjugate gradient energy minimization with no applied stress allows the screw dislocation to dissociate in its ACD glide plane and the loop to relax.

We consider Frank loops of different shapes and sizes. Hexagonal loops with edges along either $\langle1\,1\,0\rangle$ directions or $\langle1\,2\,1\rangle$ directions are considered. These two idealized morphologies have been observed in irradiated FCC materials: loops with $\langle1\,1\,0\rangle$ edges are observed for example in copper and gold crystals [17] while loops with $\langle1\,2\,1\rangle$ edges are observed in austenitic steels and nickel [11,18]. In the case of the present nickel interatomic potential, $\langle1\,2\,1\rangle$ loops have an energy lower than the corresponding $\langle1\,1\,0\rangle$ loops, but the energy difference is less than 10% and both types of loops are stable at 100 K. We therefore consider both in order to study the influence of the shape of the loops.

We consider loops with diameters of 6 or 10 nm containing, respectively, 469 and 1261 interstitial atoms in the case of $\langle1\,1\,0\rangle$ loops and 421 and 1189 interstitial atoms in the case of $\langle1\,2\,1\rangle$ loops. Given the cell dimensions used here, their density is of 150×10^{21}, 80×10^{21} and 50×10^{21} m^{-3} in the small, medium and large cells, respectively. Both loop dimensions and densities are representative of saturation values obtained experimentally at low temperatures in FCC materials [1–4].

The Frank loops may lie in either of the four families of $\{1\,1\,1\}$ planes of the crystal. We consider here loops lying in an ABD plane with a $\mathbf{C\gamma}$ Burgers vector. Because of the symmetries of the crystallography, this situation is equivalent to the case where the loop lies in a BCD plane. Similarly, whether the dislocation has an **AC** or a **CA** Burgers vector leads to equivalent configurations. Other configurations will be detailed in a future paper along with configurations involving edge dislocations.

2.3. Visualization method

Simulation results are visualized using a geometrical method. The local environment of each atom in the cell is compared to a perfect FCC environment by counting the number of first neighbors that are at less than $0.3b$ (b being the first neighbor distance) from first neighbor positions in a perfect FCC crystal. The atoms shown are those not having 12 FCC first-neighbors.

This method allows identifying the crystalline defects considered in the simulations: atoms in dislocation cores

have 10 or 11 FCC first neighbors; stacking faults appear as double layers of atoms with nine FCC first neighbors, while Frank faults appear as triple layers of atoms with six and nine FCC first neighbors.

3. Simulation results

3.1. Initial interaction mechanism

Fig. 3(a) shows the initial configuration seen from above, in the negative Z-direction, obtained after a conjugate gradient minimization with no applied stress, in the case of a 6-nm loop in an *ABD* plane centered on the glide plane of the dislocation. Atoms in the stacking faults of the dislocation and of the loop are clearly visible. The dislocation is in point-like contact with the loop and is locally constricted. Fig. 3(b) is the corresponding Burgers vector configuration. The loop edges are labeled e1–e6; these notations will be used below to explain the interaction process.

The dislocation is forced to further interact with the loop by application of a shear stress of −150 MPa. The starting reaction is shown in Fig. 4(a): the screw dislocation locally cross-slips from its initial *ACD* glide plane in an *ABC* plane where it combines with the edge e6 of the loop, to form a **γA** segment, according to the reaction: $\mathbf{CA} + \boldsymbol{\gamma}\mathbf{C} = \boldsymbol{\gamma}\mathbf{A}$. This reaction is possible because the edge e6 is contained in a $\{1\,1\,1\}$ *ABC* plane. The **γA** segment is a D-Shockley partial since it is not dissociated and adjoins the interstitial Frank fault.

In Fig. 4(b), the **γA** segment is mobile and sweeps the loop surface, removing the fault. This reaction is accompanied by a second cross-slip of the **CA** segment into the *ACD* plane which contains the edge e5. The resulting segment, dissociated in an *ACD* plane, is visible in Fig. 4(b) at the bottom of the loop. The screw dislocation has therefore locally double cross-slipped.

The D-type **γA** partial continues to sweep the loop surface, leading to the formation of a non-dissociated segment visible in Fig. 4(c). The glide plane of this segment contains both the *CA*-direction of the Burgers vector and the *BD*-direction of the edge e4 (see the Thompson tetrahedron of Fig. 1(b)). It is therefore a $\{0\,0\,1\}$ plane (we will refer to this type of dislocation as $a/2\langle 1\,1\,0\rangle\{0\,0\,1\}$ dislocations; in the special case of the edge orientation, they are called Lomer dislocations). Simultaneously, the screw dislocation combines with the edge e1 to form another $a/2\langle 1\,1\,0\rangle\{0\,0\,1\}$ segment. Finally, as the **γA** segment finishes to sweep the loop, it forms two dissociated segments along edges e2 and e3.

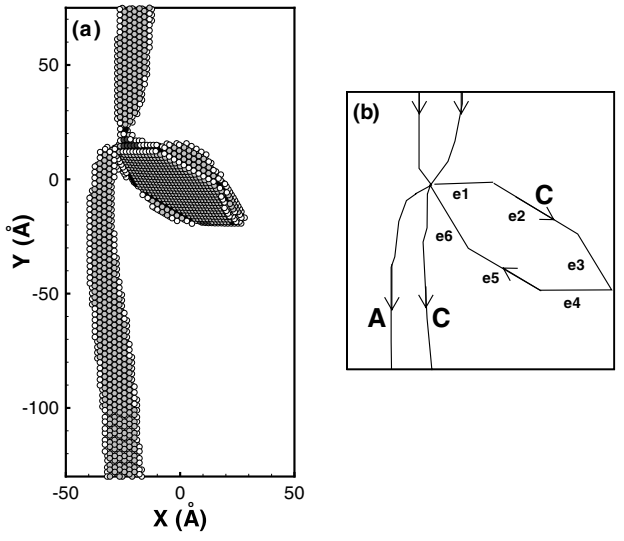

Fig. 3. Relaxed configuration. (a) Central part of the cell showing the atoms in the stacking faults of the dislocation and the Frank loop and (b) corresponding Burgers vector configuration. The color of the atoms scales with their number of FCC first neighbors.

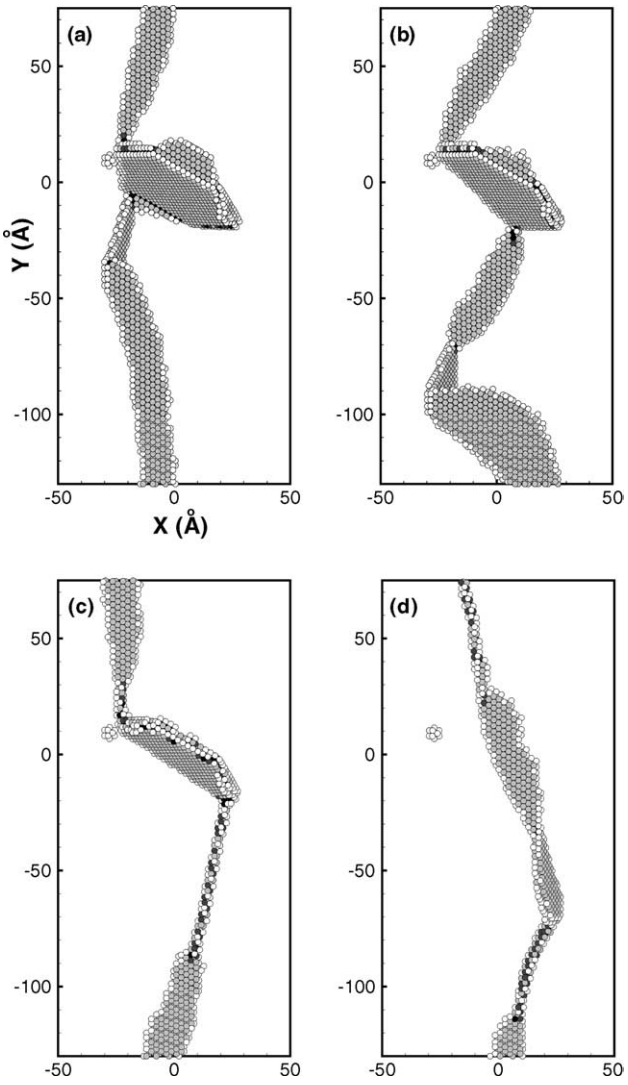

Fig. 4. Unfaulting reaction at different times after application of a stress $\sigma_{yz} = -150$ MPa: (a) 10 ps, (b) 15 ps, (c) 25 ps and (d) 32 ps.

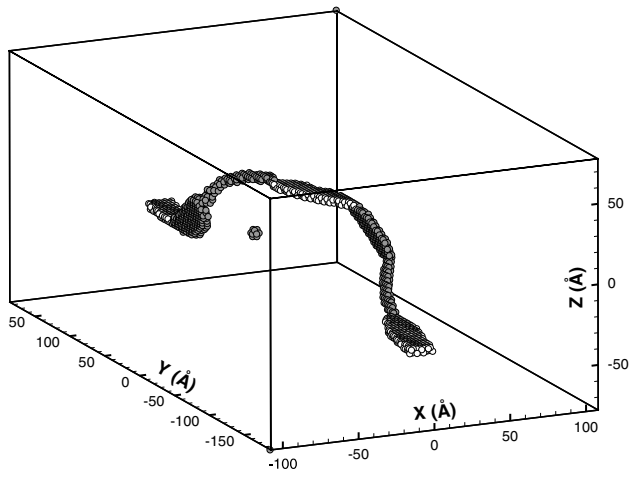

Fig. 5. Final configuration. The segments dissociated in *ACD* planes are shown in white; the superjogs are in gray.

The final structure is shown in Fig. 4(d) from above and in Fig. 5 in 3D perspective. It corresponds to a 'helical turn' made of both dissociated $a/2\langle 1\,1\,0\rangle\{1\,1\,1\}$ and non-dissociated $a/2\langle 1\,1\,0\rangle\{0\,0\,1\}$ segments. It has inherited the hexagonal shape of the initial Frank loop.

Note that the isolated cluster of atoms visible in Fig. 4(d) corresponds to a vacancy produced at the beginning of the reaction.

The helical turn is better interpreted as two screw segments dissociated in *ACD* planes, linked by superjogs each made of a glissile segment (dissociated in an *ABC* plane) and a constricted segment in a $\{0\,0\,1\}$ plane. In order to illustrate this point, in Fig. 5, atoms in the stacking faults of the screw segments are shown in white and atoms in the superjogs in gray. Simulations performed in the larger cell show that the extension of the superjogs is independent of the cell size; the superjogs have the same extension in the *Y*-direction and the dissociated segments are longer.

3.2. Resistance of the structure

The helical turn is sessile because it is made of segments with glide planes parallel to the dislocation line. Moreover, the superjogs contain $a/2\langle 1\,1\,0\rangle\{0\,0\,1\}$ dislocations which have a low mobility.

We performed simulations with increasing applied stress in the three simulation cells in order to evaluate the unpinning stress of the dislocation as a function of the distance between defects. The result is shown in Fig. 6 with triangles. It will be discussed in Section 4.

Fig. 7 shows the unpinning reaction. It involves an Orowan process of the segment dissociated in the upper *ACD* plane: as this segment bows out, it pushes the superjogs towards each other (Figs. 7(a) and (b)) until both arms of the dislocation join (Fig. 7(c)). The dislocation then unpins and leaves behind a perfect prismatic loop (Fig. 7(d)). The net result of the interaction is therefore the unfaulting of the loop and its transformation into a perfect loop.

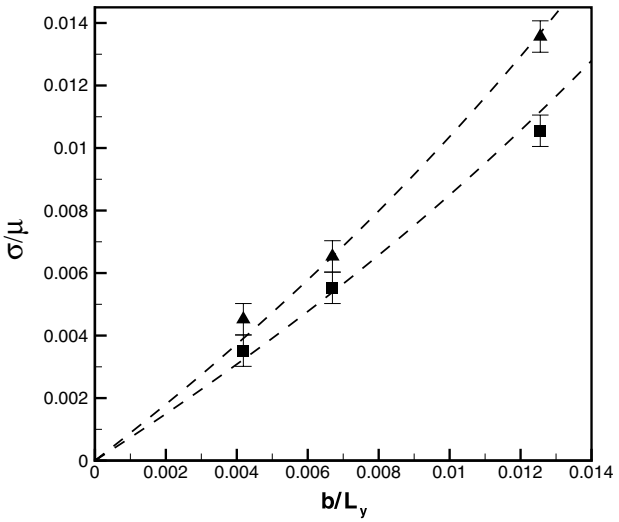

Fig. 6. Unpinning stress σ as a function of the inverse of the length of the simulation cell along the dislocation line L_y. Triangles correspond to $\langle 1\,1\,0\rangle$ loops, squares to $\langle 1\,2\,1\rangle$ loops. $\mu = 74,600$ MPa is the shear modulus in $\{1\,1\,1\}$ planes, $b = 2.5$ Å is the Burgers vector. Dashed lines are the Orowan stress predicted from elasticity theory (see text).

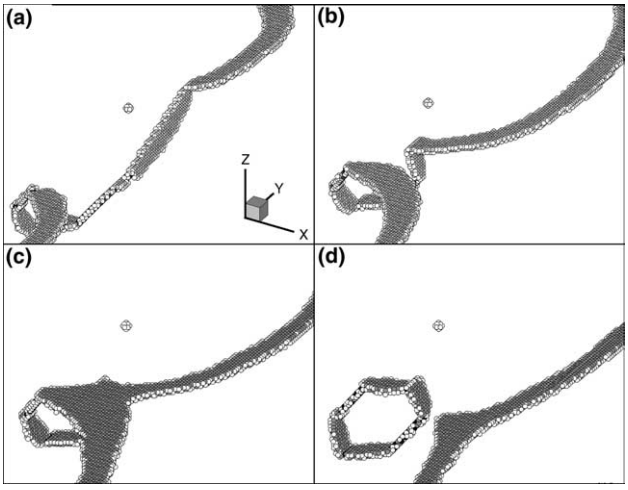

Fig. 7. Unpinning reaction at different times after application of stress $\sigma_{yz} = -600$ MPa: (a) 18 ps, (b) 24 ps, (c) 25.2 ps and (d) 27 ps.

3.3. Influence of the shape of the loop

The unfaulting reaction described above is expected to depend on the shape of the loop because it involves recombinations of the dislocation with loop edges lying in $\{1\,1\,1\}$ planes. In order to investigate this point, we considered hexagonal loops with edges in $\langle 1\,2\,1\rangle$ directions, as observed, for example, in austenitic steels [11,18].

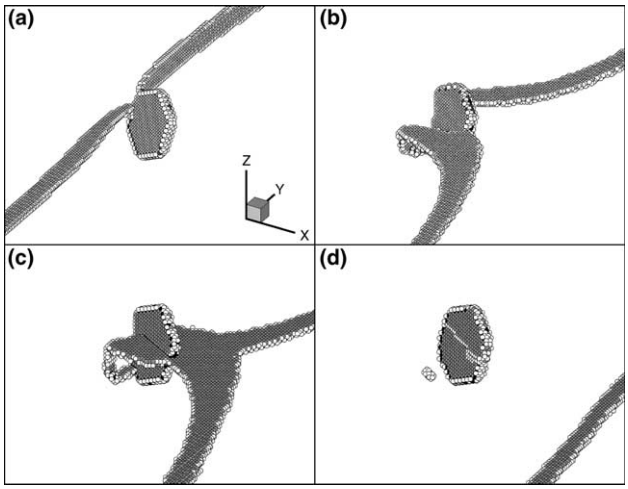

Fig. 8. Case of a $\langle 1\,2\,1\rangle$ loop: (a) relaxed configuration at zero stress; configurations at $\sigma_{yz} = -300$ MPa at times: (b) 19.8 ps, (c) 24.6 ps and (d) 28.2 ps.

Fig. 8(a) shows the relaxed configuration in the large simulation cell after a conjugate gradient minimization with no applied stress. During the relaxation, the dislocation came into contact with the loop and got locally constricted. It did not further react with the loop but instead, a constricted node was emitted on the right-hand side, inducing a cross-slip of the screw dislocation. This can be seen in Fig. 8(a), where the right-hand arm of the dislocation is now in an *ABC* plane.

Upon application of an increasing shear stress, the arms of the dislocation bow out and force the constricted node to come back into contact with the loop (Fig. 8(b)). The cross-slipped arm therefore comes back into its initial *ACD* plane. On the left-hand side of the loop, the dislocation cross-slips to form a D-Shockley partial. Since the edge of the loop is not in a $\{1\,1\,1\}$ plane, the cross-slipped segment of the screw dislocation is neither in a $\{1\,1\,1\}$ plane, and is thus not dissociated. This structure is stable presumably because further unfaulting of the loop would require the cross-slip of the screw dislocation in planes different from $\{1\,1\,1\}$ planes, which is unfavorable.

At $\sigma_{yz} = -300$ MPa, the dislocation unpins by an Orowan process: the left-hand arm comes into contact, first with the loop (Fig. 8(b)), then with the right-hand arm (Fig. 8(c)). The dislocation unpins and leaves behind a loop which is sheared (Fig. 8(d)). A step is visible on the loop as a line of white atoms.

We evaluated the unpinning stress of the dislocation as a function of the size of the cell, shown in Fig. 6 as squares.

4. Discussion

We considered a configuration close to the one observed in TEM by Strudel and Washburn [8] in quenched aluminum. By way of contrast with TEM, MD simulations offer full atomic detail of the interaction process and allow the evaluation of the resistance due to the defect. Moreover, the irradiation defects may be simulated with realistic dimensions and densities.

The boundary conditions presented here allow the simulation of screw dislocations in an infinite periodic glide plane without simulating a dipole, thus leading to smaller simulation cells. With the corresponding boundary conditions for edge dislocations presented in [13], the influence of the dislocation character on atomic scale processes may be studied. One limitation of this type of boundary conditions is that, since the simulation cells are relatively small, the dislocations can rotate only locally and are forced to keep on average their initial character, which constraints their motion. For example, in the present case, the helical turn is a strong obstacle to the motion of the screw dislocation, but, if the dislocation was able to rotate, it would be a weak obstacle for an edge dislocation that could drag both superjogs in a way similar to the one considered in [13].

We studied the formation of a helical turn. The critical reaction for unfaulting is a local cross-slip of the screw dislocation, which occurs within a short time scale at low temperature (100 K). It is not thermally activated but controlled by the gain in energy related to the recombination of the cross-slipped segment with the loop edge. Athermal cross-slip is also observed in the case of $\langle 1\,2\,1\rangle$ loops with the emission of a constricted node from the loop. This point is important because cross-slip traces are observed by TEM during the formation, thickening and branching of the clear bands, even at the temperature of liquid helium [6,7,12]. The present simulations show that these cross-slip events are promoted by the short-range core interactions between the moving dislocations and the Frank loops, leading to a local constriction of the dislocation and athermal cross-slip.

The simulations confirm the existence of D-Shockley partials which have the particularity to have a core extended over two adjacent $\{1\,1\,1\}$ planes. In other configurations not presented here (in particular when the Frank loop is in a cross-slip plane of the screw dislocation), unfaulting involves sweeping by two successive and separate Shockley partials. Therefore, both types of dislocations (single D-type partial or two Shockley partials) are possible, their occurrence depending on the configuration.

The present study also insists on the importance of the shape of the Frank loops. Loops with edges along $\langle 1\,2\,1\rangle$ directions are not unfaulted but sheared. The reason is that unfaulting requires several cross-slips and recombinations of the screw dislocation with edges of the loop. In the present simulations, after unpinning of the dislocation, the fault of the sheared $\langle 1\,2\,1\rangle$ loop is fully reconstructed because the D-Shockley is mobile and glides back. In materials where the dislocations are

less mobile, as in alloys, the D-Shockley may not glide back, leading to a partially unfaulted loop. Moreover, a loop cut by several dislocations, as in the case of a shear band, will end up being separated in halves. Both cases (partially unfaulted loops and loops cut in halves) have indeed been observed by Suzuki et al. [11] in austenitic steels where the authors identified the loops as having $\langle 1\,2\,1\rangle$ edges. We should note that unfaulting depends on the configuration: loops lying in a cross-slip plane of the screw dislocation are unfaulted independently of their shape. Therefore, in materials with $\langle 1\,1\,0\rangle$ loops, all contact reactions lead to unfaulting, while, in materials with $\langle 1\,2\,1\rangle$ loops, it depends on the configuration.

Materials with $\langle 1\,1\,0\rangle$ loops are expected to soften and acquire clear bands because the perfect prismatic loops are weak obstacles that can be eliminated by prismatic glide or drag by the moving dislocations [6]. Materials with $\langle 1\,2\,1\rangle$ loops are also expected to soften, in much the same way as alloys with shearable precipitates [7]. However, in this latter case, the clear bands will be 'less clear' since the loops will have to be cut down to atomic sizes before being absorbed by the moving dislocations. Indeed, simulations performed with small Frank loops, containing less that 20 interstitials, show that these loops are unstable in presence of a dislocation: they transform spontaneously into perfect glissile loops with a $a/2\langle 1\,1\,0\rangle$ Burgers vector and are absorbed in the core of the dislocation and dragged in the same way as shown in [13]. This is consistent with the observations of Suzuki et al. [11] who reported a localization of the deformation in shear bands which contained a large number of debris.

Fig. 6 shows the unpinning stress for $\langle 1\,1\,0\rangle$ and $\langle 1\,2\,1\rangle$ loops as a function of the length of the cell along the dislocation line. Since in both cases unpinning involves an Orowan looping, we compared these stresses with the expression obtained by Scattergood and Bacon [19] for such a process:

$$\frac{\sigma}{\mu}=\frac{1}{2\pi(1-\nu)}\frac{b}{L}\left(-\ln\left(\frac{b}{D}+\frac{b}{L}\right)+B\right), \tag{3}$$

where $\mu = 74,600$ MPa is the shear modulus in $\{1\,1\,1\}$ planes, $b = 2.5$ Å is the Burgers vector, $\nu = 0.33$ is the Poisson ratio, D is the size of the obstacle and $L = L_y - D$ is the spacing between obstacles. This expression was obtained from a continuum model simulation of a dislocation in an anisotropic medium passing through a row of either voids or impenetrable precipitates. In the latter case, which corresponds best to our simulations, they found $B = 0.615$.

We fitted the effective size of the obstacles in our simulations using the above expression and found for $\langle 1\,2\,1\rangle$ loops, $D = 3.2 \pm 0.1$ nm and $\langle 1\,1\,0\rangle$ loops, $D = 5.3 \pm 0.3$ nm. These sizes are close to the real size of the loops but are effective because: (1) Eq. (3) was obtained using spherical obstacles with no elastic fields, (2) the $\langle 1\,2\,1\rangle$ loops are seen from the side and their effective size is increased by the sessile cross-slipped segment on the left-hand side of the loop (Fig. 8(b)) and (3) the size of the helical turn, which is the distance between the superjogs, varies during the interaction (D being this distance when the dislocation bowing out becomes unstable). The good fit of the simulation results with Eq. (3) shows that the critical unpinning stress is controlled by the bowing out of the dislocation and not the elastic interaction between the dislocation and the defect.

5. Conclusion

MD simulations have been used to study the interaction between a screw dislocation and a Frank loop which does not lie in its cross-slip plane. The key results are:

(1) Short-range core interactions between the dislocation and the loop promote local constrictions and athermal cross-slips.
(2) The shape of the loops controls whether the loops are unfaulted or sheared, which explains TEM observations made by Suzuki et al. in irradiated austenitic steels.
(3) The Frank loops are strong obstacles with unpinning reactions involving Orowan processes.

We are currently completing the study in pure nickel by considering the other possible configurations, involving both edge and screw dislocations. The next step will then be to consider alloying effects and, in particular, their influence on the mobility of the dislocations and the stability of the faults.

Acknowledgements

This work was supported by the Institut National Polytechnique de Grenoble. The author thank Dr. Cédric Pokor and Pr. Yves Bréchet, whose work motivated the present study, as well as Dr. Marc Fivel and Dr. Marc Verdier for fruitful discussions.

References

[1] Singh BN, Zinkle SJ. J Nucl Mater 1993;206:212.
[2] Zinkle SJ, Snead LL. J Nucl Mater 1995;225:123.
[3] Maziasz PJ. J Nucl Mater 1993;205:118.
[4] Zinkle SJ, Maziasz PJ, Stoller RE. J Nucl Mater 1993;206:266.
[5] Lucas GE. J Nucl Mater 1993;206:287.
[6] Sharp JV. Philos Mag 1967;16:77.
[7] Luft A. Progr Mater Sci 1991;35:97.
[8] Strudel JL, Washburn J. Philos Mag 1964;9:491.
[9] Kuhlmann-Wilsdorf D. Philos Mag 1958;49:125.
[10] Weertman J, Weertman JR. Elementary dislocation theory. London: Macmillan; 1967. p. 99.

[11] Suzuki M, Sato A, Mori T, Nagakawa J, Yamamoto N, Shiraishi H. Philos Mag A 1992;65:1309.
[12] Robach JS, Robertson IM, Wirth BD, Arsenlis A. Philos Mag 2003;83:955.
[13] Rodney D, Martin G. Phys Rev Lett 1999;82:3272;
Rodney D, Martin G. Phys Rev B 2000;61:8714;
Rodney D, Martin G, Bréchet Y. Mater Sci Eng A 2001;309–310:198.
[14] Wirth BD, Bulatov VV, Diaz de la Rubia T. J Eng Mater Technol 2002;124:329.
[15] Osetsky Yu N, Bacon DJ, Mohles V. Philos Mag; 2003 [in press].
[16] Angelo JE, Moody NR, Baskes MI. Model Simul Mater Sci Engrg 1995;3:289.
[17] Kiritani M, Takata H. J Nucl Mater 1978;69–70:277.
[18] Boulanger L, Soisson F, Serruys Y. J Nucl Mater 1996;233:1004.
[19] Scattergood RO, Bacon DJ. Acta Metall 1982;30:1665.